Variable pitch spring for nonlinear energy sink: Application to passive vibration control

Donghai Qiu, Manuel Paredes, Sébastien Seguy

Variable pitch spring for nonlinear energy sink: application to passive vibration control

Donghai Qiu[1], Manuel Paredes[1] and Sébastien Seguy[1]

Abstract

This paper aims to propose a generalized methodology for designing a novel Nonlinear Energy Sink (NES) with variable pitch springs. To this end, a generic model of the NES system providing the nonlinearity of pure cubic stiffness is introduced. Key features of the model include: (i) specifically sizing two variable pitch springs to provide the force polynomial components with only linear and cubic terms; (ii) pre-compressing two springs at the transition point to produce smooth nonlinear force characteristics; (iii) adding a negative stiffness mechanism to counterbalance the linear term. To generate the variable pitch spring, design parametrization is implemented. The type of shape and the pitch distribution adopted for the spring are shown to fit the objective force-displacement function well. To validate the concept, a special sized NES system is developed. Identification of the force-displacement relation and experiments for the whole system embedded on an electrodynamic shaker are studied. The results show that this NES can not only output the anticipated nonlinearity, but can also produce energy pumping to protect the primary system in a large band of frequencies, thus making it practical for the application of passive vibration control.

Keywords

Variable pitch spring, Cubic stiffness, Nonlinear energy sink, Negative stiffness mechanism, Passive vibration control

Nomenclature

$\bar{n}_i$	number of coils of the i_{th} spring group
ϵ	mass ratio between NES and linear oscillator
λ_1, λ_2	reduced damping of linear oscillator and NES
a_1, a_3	linear and cubic stiffness at the nonlinear regime
c_1, c_2	damping of linear oscillator and NES
D	mean diameter of variable pitch spring
d	wire diameter of variable pitch spring
G	amplitude of the harmonic excitation
K	reduced nonlinear stiffness of NES
k	stiffness of the linear spring
k_0	stiffness at the linear regime
k_1, k_2	stiffness of linear oscillator and NES
l	remaining length of pre-compressed spring
l_0	free length of linear spring
L_f	free length of variable pitch spring
l_p	pre-compressed length of linear spring
m_1, m_2	mass of linear oscillator and NES
n	number of spring groups in nonlinear regime
n_a	number of active coils of variable pitch spring
P_t, s_t	force and displacement of the transition point
t_i	pitch of the i_{th} spring group
x, y	displacement of linear oscillator and NES
x_e	imposed harmonic displacement

1 Introduction

Over recent decades, nonlinear vibration absorbers have advanced rapidly and show considerable potential in passive vibration control applications [1]. Particularly in the areas of aero-space and civil engineering, absorbers are required to be light and to work over a broad spectrum of frequencies, leading to increased interests in exploiting the absorber with different nonlinearities (e.g. vibro-impact, monostable duffing, non-polynomial and bistable oscillators) [2–8]. Among such devices, the nonlinear absorber with cubic stiffness, also called the Nonlinear Energy Sink (NES), has proved to be effective for moderate-energy vibration mitigation [1]. This type of absorber is characterized by a secondary mass strongly coupled via a cubic stiffness to the primary system that needs to be protected [9]. Because of the nonlinearity, irreversible Targeted Energy Transfer (TET) takes place from the main structure to the secondary mass, enabling the NES to be effective in a broad band of frequencies.

Targeted Energy Transfer mechanisms and the feasibility of NES in different applications have been analyzed in detail by [10–15]. In these approaches, the essential cubic stiffness was mostly achieved by adopting a construction of two linear

[1]Institut Clément Ader (ICA), CNRS, INSA-ISAE-Mines Albi-UPS, Université de Toulouse, 3 rue Caroline Aigle, Toulouse, F-31400, France

Corresponding author:
Donghai Qiu, Institut Clément Ader (ICA), CNRS, INSA-ISAE-Mines Albi-UPS, Université de Toulouse, 3 rue Caroline Aigle, Toulouse, F-31400, France.
Email: donghai.qiu@insa-toulouse.fr

springs with no pretension (e.g. a beam [16], a piano wire [17], a membrane [18] and helical springs [19]). Because of their self-geometric nonlinearity, the springs stretch in tension, thus creating the cubic force. However, this classical type of device cannot effectively take advantage of spring compression and tension, and the result is a large vertical structure attached to the main system. Addition of a relatively weak nonlinear stiffness existing at the beginning extension, leads to the whole cubic term being approximated to a linear term. Thus, implementing cubic stiffness elements in practice is still an important issue if the application of NES is to be broadened.

Nowadays, physical determination of the nonlinear force-displacement characteristics can be performed by two common methods. One is direct using nonlinear springs, such as conical springs, variable pitch springs, piecewise stiffness springs, and special sized beam segments [20–24]. Various applications of these springs can be found in robotic joints, bandpass filters, vehicle suspensions and crashworthiness structures. The other method is to design a mechanism with variable stiffness. For example, Wu and Lan [25] proposed a linear variable stiffness mechanism with preloaded curved beams. Sönmez and Tutum [26] introduced a compliant bistable mechanism with flexible beams. Chen and Lan [27] designed an adjustable constant force mechanism for adaptive end effector operations. Stanton et al. [28] developed a piezoelectric cantilever with a permanent magnet for the energy harvesting system. For these methods, a key issue to be satisfied for a NES is that the linear part of the force-displacement characteristics should be very small so as to ensure that the NES can adapt itself to the frequency of any primary system [29]. Whether it is possible to combine the advantage of nonlinear springs and variable stiffness mechanisms, so as to obtain strongly cubic stiffness without any linear part for the NES system. With this in mind, a generalized methodology for designing a novel NES with the proposed components is presented in this paper.

The structure of the paper is as follows. The first section is devoted to develop the generic model of the NES system, including the dynamical model for targeted energy transfer and the physical configuration. The next section provides a design theory of variable pitch spring under a given force-displacement function. In the third section, the designed springs and NES system are identified, and experiments for the whole system embedded on an electrodynamic shaker are performed. Finally, some concluding remarks are proposed.

2 Generic model of NES system

2.1 Dynamical model of NES system

The dynamic model of the NES system presented here is based on [19] and [30]. The system is composed of a harmonically excited linear oscillator (LO) strongly coupled with a cubic NES (see Fig. 1) and is described by the following equations of motion:

$$\begin{cases} m_1\ddot{x} + k_1 x + c_1\dot{x} + c_2\left(\dot{x}-\dot{y}\right) + k_2\left(x-y\right)^3 \\ = k_1 x_e + c_1\dot{x}_e \\ m_2\ddot{y} + c_2(\dot{y}-\dot{x}) + k_2\left(y-x\right)^3 = 0 \end{cases} \tag{1}$$

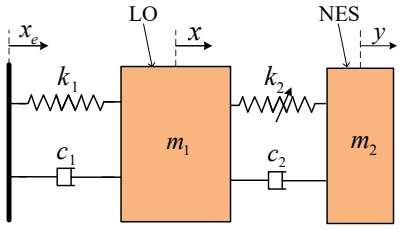

Figure 1. Schematic of a harmonically excited LO coupled with a cubic NES

where x, m_1, c_1, k_1 and y, m_2, c_2, k_2 are the displacement, mass, damping and stiffness of the LO and the cubic NES respectively and the dots denote differentiation with respect to time. The imposed harmonic displacement x_e is expressed as: $x_e = G\cos(\omega t)$.

Substituting $k_1 = m_1\omega_0^2$, $t = \tau/\omega_0$ and $\omega = \Omega\omega_0$ to equations (1):

$$\begin{cases} \ddot{x} + x + \frac{c_1}{m_1\omega_0}\dot{x} + \frac{c_2}{m_1\omega_0}(\dot{x}-\dot{y}) + \frac{k_2}{m_1\omega_0^2}(x-y)^3 \\ = Gcos(\Omega\tau) - \frac{c_1\Omega}{m_1\omega_0}Gsin(\Omega\tau) \\ \frac{m_2}{m_1}\ddot{y} + \frac{c_2}{m_1\omega_0}(\dot{y}-\dot{x}) + \frac{k_2}{m_1\omega_0^2}(y-x)^3 = 0 \end{cases} \tag{2}$$

Then introducing $c_1 = \lambda_1 m_2\omega_0$, $c_2 = \lambda_2 m_2\omega_0$ and $k_2 = m_2\omega_0^2 K$ to Eqs. (2):

$$\begin{cases} \ddot{x} + x + \frac{\lambda_1 m_2}{m_1}\dot{x} + \frac{\lambda_2 m_2}{m_1}(\dot{x}-\dot{y}) + \frac{Km_2}{m_1}(x-y)^3 \\ = Gcos(\Omega\tau) - \frac{\lambda_1 m_2\Omega}{m_1}Gsin(\Omega\tau) \\ \frac{m_2}{m_1}\ddot{y} + \frac{\lambda_2 m_2}{m_1}(\dot{y}-\dot{x}) + \frac{Km_2}{m_1}(y-x)^3 = 0 \end{cases} \tag{3}$$

Substituting $m_2/m_1 = \epsilon$ and $G = \epsilon F$ to Eqs. (3):

$$\begin{cases} \ddot{x} + x + \epsilon\lambda_1\dot{x} + \epsilon\lambda_2\left(\dot{x}-\dot{y}\right) + \epsilon K\left(x-y\right)^3 \\ = \epsilon F\cos\Omega\tau - \epsilon^2 F\lambda_1\Omega sin(\Omega\tau) \\ \epsilon\ddot{y} + \epsilon\lambda_2\left(\dot{y}-\dot{x}\right) + \epsilon K\left(y-x\right)^3 = 0 \end{cases} \tag{4}$$

where the term containing ϵ^2 is so small that it can be eliminated. The system of equations (1) can be finally reduced to the dimensionless form:

$$\begin{cases} \ddot{x} + x + \epsilon\lambda_1\dot{x} + \epsilon\lambda_2\left(\dot{x}-\dot{y}\right) + \epsilon K\left(x-y\right)^3 = \epsilon F\cos\Omega\tau \\ \epsilon\ddot{y} + \epsilon\lambda_2\left(\dot{y}-\dot{x}\right) + \epsilon K\left(y-x\right)^3 = 0 \end{cases} \tag{5}$$

The corresponding physical parameters of rescaling process are expressed as follows:

$$\epsilon = \frac{m_2}{m_1},\quad {\omega_0}^2 = \frac{k_1}{m_1},\quad K = \frac{k_2}{m_2{\omega_0}^2},\quad \lambda_1 = \frac{c_1}{m_2\omega_0},\quad \lambda_2 = \frac{c_2}{m_2\omega_0},\quad F = \frac{G}{\epsilon},\quad \Omega = \frac{\omega}{\omega_0},\quad \tau = \omega_0 t \tag{6}$$

New variables representing the displacement of the centre of mass and the internal displacement of the cubic NES are introduced as follows:

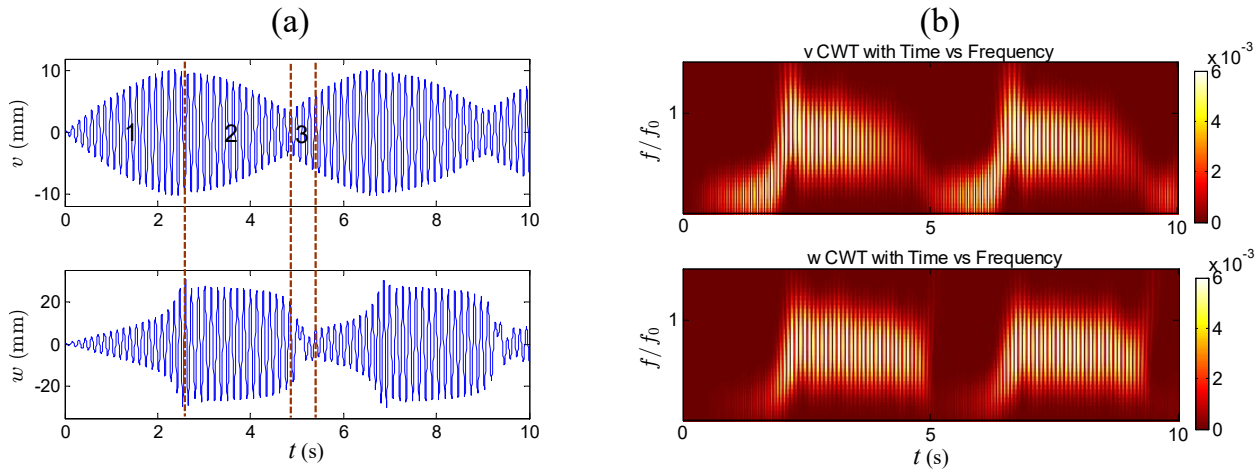

Figure 2. Cubic NES under periodic forcing with parameters $K = 2400$, $\lambda_1 = 0.8$, $\lambda_2 = 0.2$, $\epsilon = 0.015$, $G = 0.3\,mm$ and initial conditions $x_0 = 0$, $\dot{x}_0 = 0$, $y_0 = 0$ and $\dot{y}_0 = 0$. (a) time-displacement of LO and NES; (b) wavelet transform of LO and NES. The states of 1, 2 and 3 represent the regime of nonlinear beating, transient resonance capture and escape from resonance capture, respectively.

$$v = x + \epsilon y, \quad w = x - y \tag{7}$$

Substituting Eqs. (7) into Eqs. (5):

$$\begin{cases} \ddot{v} + \epsilon\lambda_1 \dfrac{\dot{v} + \epsilon\dot{w}}{1+\epsilon} + \dfrac{v + \epsilon w}{1+\epsilon} = \epsilon F \cos\Omega\tau \\ \ddot{w} + \epsilon\lambda_1 \dfrac{\dot{v} + \epsilon\dot{w}}{1+\epsilon} + \dfrac{v + \epsilon w}{1+\epsilon} + \lambda_2 (1+\epsilon)\,\dot{w} + K(1+\epsilon)\,w^3 \\ = \epsilon F \cos\Omega t \end{cases} \tag{8}$$

The system is studied in the vicinity of the 1:1 resonance, where both the LO and the NES execute time-periodic oscillations with identical frequency Ω. To obtain the analytical periodic solution, two new complex variables are introduced:

$$\phi_1 e^{i\Omega\tau} = \dot{v} + i\Omega v, \quad \phi_2 e^{i\Omega\tau} = \dot{w} + i\Omega w \tag{9}$$

Substituting Eqs. (9) into Eqs. (8) and keeping only the secular term containing $e^{i\Omega\tau}$ yields the following slowly modulated system:

$$\begin{cases} \dot{\phi}_1 + \dfrac{i\Omega}{2}\phi_1 + \dfrac{\epsilon\lambda_1(\phi_1 + \epsilon\phi_2)}{2(1+\epsilon)} - \dfrac{i(\phi_1 + \epsilon\phi_2)}{2\Omega(1+\epsilon)} - \dfrac{\epsilon F}{2} = 0 \\ \dot{\phi}_2 + \dfrac{i\Omega}{2}\phi_2 + \dfrac{\epsilon\lambda_1(\phi_1 + \epsilon\phi_2)}{2(1+\epsilon)} - \dfrac{i\,(\phi_1 + \varepsilon\phi_2)}{2\Omega(1+\epsilon)} - \dfrac{\epsilon F}{2} \\ + \dfrac{\lambda_2(1+\epsilon)\phi_2}{2} - \dfrac{3iK\,(1+\epsilon)\,\phi_2^2\bar{\phi}_2}{8\Omega^3} = 0 \end{cases} \tag{10}$$

In the context of energy pumping, the mass ratio ϵ is taken to be small ($\approx 1\%$). In this case, Eq. (10) can be analysed by a perturbation method with respect to this small parameter. For this purpose, the method of multiple scales [31, 32] is introduced in the following form:

$$\begin{aligned} \phi_i = \phi_i(\tau_0, \tau_1, + \ldots), \quad & \frac{d}{d\tau} = \frac{\partial}{\partial\tau_0} + \epsilon\frac{\partial}{\partial\tau_1} + \cdots \\ \tau_k = \epsilon^k\tau, \quad & k = 0, 1, \ldots \end{aligned} \tag{11}$$

Substituting Eqs. (11) into Eqs. (10) and equating coefficients of ϵ^0 gives:

$$\begin{aligned} & \frac{\partial}{\partial\tau_0}\phi_1 = 0 \\ & \frac{\partial}{\partial\tau_0}\phi_2 + \frac{\lambda_2}{2}\phi_2 + \frac{i}{2}(\phi_2 - \varphi_1) - \frac{3iK}{8}\phi_2^2\,|\phi_2| = 0 \end{aligned} \tag{12}$$

Then we introduce the new variables as follows:

$$\phi_1(\tau_1) = N_1 e^{i\theta_1}, \quad \phi_2(\tau_1) = N_2 e^{i\theta_2} \tag{13}$$

With this change of variables in Eqs. (12), a topological structure of slow invariant manifold (SIM) is obtained in the following form:

$$N_{10}^2 = (1 + \lambda_2^2)N_{20}^2 - \frac{3K}{2}N_{20}^4 + \frac{9K^2}{16}N_{20}^6 \tag{14}$$

where N_{10}, N_{20} correspond to the amplitude of LO and NES in slow time scale, respectively. According to [33], the SIM structure admits two extrema (N_{21} and N_{22}) and can be divided into two stable branches and one unstable branch, where the unstable branch of the SIM is mainly responsible for the possible occurrence of energy pumping and may give rise to the strongly modulated response (SMR).

To illustrate this mechanism, a strongly modulated response and its corresponding wavelet transform are presented in Fig. 2. A quasi-periodic response with slow variation of the amplitudes of both oscillators is observed. In this regime, the procedure of energy pumping can be classified as follows: (1) nonlinear beating, where a small amplitude of NES corresponds to the growth of LO amplitude; (2) transient resonance capture, with the frequency component of 1:1 resonance (see Fig. 2(b)), in this case large targeted energy is extracted and dissipated by NES, leading to a fast decrease of the LO amplitude; (3) escape from resonance capture, in which the NES crosses the bifurcation and is quickly attracted to the low branch of SIM (see Fig. 3), which leads to a jump down for the energy

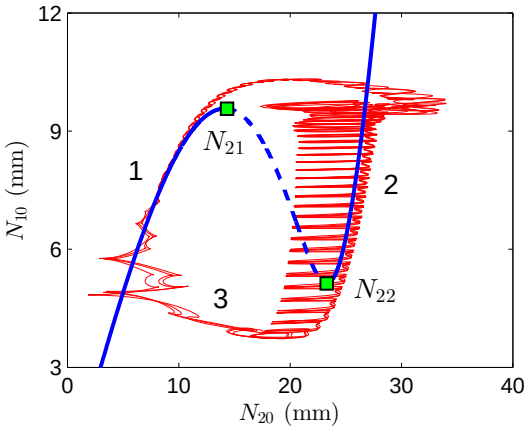

Figure 3. SIM structure (blue line) and the transient projection motion of SMR (red line). The states 1, 2 and 3 represent the regime of nonlinear beating, transient resonance capture and escape from resonance capture, respectively.

of the NES. This SMR regime demonstrates the irreversible targeted energy transfer from LO to NES, which suppresses energy more efficiently than a steady state response.

2.2 Physical model of NES system

The physical NES model developed in this paper is presented in Fig. 4(a). It consists of a nonlinear characteristic part and a negative stiffness mechanism. The negative stiffness mechanism is created by two linear springs hinged together at one end with the mass of the NES, while the other ends, subjected to two equivalent preloads P, are allowed to move freely in frictionless horizontal channels.

As the two linear springs are subjected only to horizontal forces, their force on the axial spring is zero. From the equilibrium position, an external force (i.e. F) is applied to generate an upward displacement (i.e. u) of the output link. Within an operating region of the linear spring, the stiffness curve depends on the preload p. The three F-u curves in Fig. 4(b) denote the NES system with different lateral preloads. The corresponding force-displacement curves of the two horizontal springs and the vertical spring are presented in Fig. 5 (b) and (d), respectively. From the curve with no preload, a positive preload decreases the linear stiffness, whereas a negative preload increases it. As can be seen from Fig. 4(b), the force characteristic of case $p < 0$ is almost dominated by its component of linear stiffness (i.e. the thick black line). Thus, to obtain strong (non-linearizable) nonlinearity, the negative stiffness mechanism with $p > 0$ is adopted.

A detailed realization of the NES system is presented in Fig. 6, where the negative stiffness mechanism is implemented by two cylindrical compression springs having free length l_0. After pre-compressing to the length l (see Fig. 6(a)), the force-displacement relation with the Taylor expansion is expressed as:

$$f_p = 2k\frac{l_p}{l}\cdot u - k\frac{(l+l_p)}{l^3}\cdot u^3 \tag{15}$$

For the axial direction, the nonlinear characteristic part is realized by two variable pitch springs. Unlike ordinary compression springs, variable pitch springs are designed to have a nonlinear spring rate. These springs can have multiple rates or a progressively increasing spring rate as the spring compresses. Since the pitch is varied, some of the coils close up faster than the rest and become inactive, meaning that they no longer absorb the compressive energy resulting from applied forces. When the amount of active energy absorbing coils is reduced, the spring becomes stiffer and the rate increases.

To benefit from the nonlinear performance of the variable pitch spring, a symmetrical connecting type of spring is proposed, as shown in Fig. 6(b). However, this configuration has a linear stiffness part that is hard to eliminate. To obtain the cubic stiffness of the NES system, the objective function of the variable pitch spring is defined as:

$$F = \begin{cases} k_0 \cdot u & (u \le s_t) \\ a_3(u-s_t)^3 + a_1(u-s_t) + P_t & (u > s_t) \end{cases} \tag{16}$$

where k_0 is the stiffness of the linear phase, a_3 is the expected cubic value, a_1 is the spring rate after the group in linear phase is fully compressed to the ground block, P_t and s_t represent the force and displacement of the transition point, respectively.

To skip the linear phase, a method of pre-compressing spring at the transition point is adopted. By changing the initial origin point, the behaviors of two variable pitch springs can belong one to the linear and one to the nonlinear regime simultaneously.

By combining the two spring curves, a composed stiffness curve is obtained and the force relation is:

$$f_K = (a_1 + k_0)\cdot u + a_3 \cdot u^3 \tag{17}$$

Obviously, the new curve is smooth and no longer piecewise (see Fig. 7). By adding the force of two variable pitch springs (i.e. f_K) to the force of the negative stiffness mechanism (i.e. f_p), the composed force of the NES system is obtained:

$$F = (a_1 + k_0 - 2k\frac{l_p}{l})\cdot u + (a_3 + k\frac{(l+l_p)}{l^3})\cdot u^3 \tag{18}$$

As can be seen from Eq. (18), if $a_1 + k_0 = 2kl_p/l$, the linear component can be counterbalanced by the negative stiffness mechanism. In this case, only the pure cubic term of the equation will be left, and its coefficient will be larger with the addition of two linear springs.

3 Design theory of variable pitch spring

Since the stiffness of a variable pitch spring is piecewise, producing a smooth and nonlinear curve like that of a conical spring is hard. Here, a method using special coordinate points to fit the required stiffness curve is adopted. Depending on the method of curve fitting, two types of shape providing the polynomial components with only linear and cubic terms are proposed: (1) each coil having a different pitch; (2) each group of coils having a different pitch (see Fig. 8). The detailed force characteristics of the two types are presented in Fig. 9. For the first type, each coil is set with a different

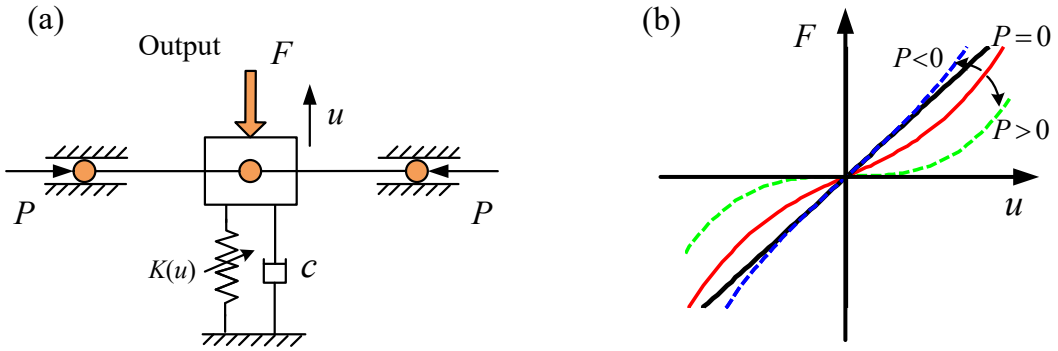

Figure 4. (a) Schematic of NES system with negative stiffness mechanism and nonlinear spring; (b) restoring force with respect to the compressing length. Where the thick black line corresponds to the component of linear stiffness for the force characteristic of case $p < 0$.

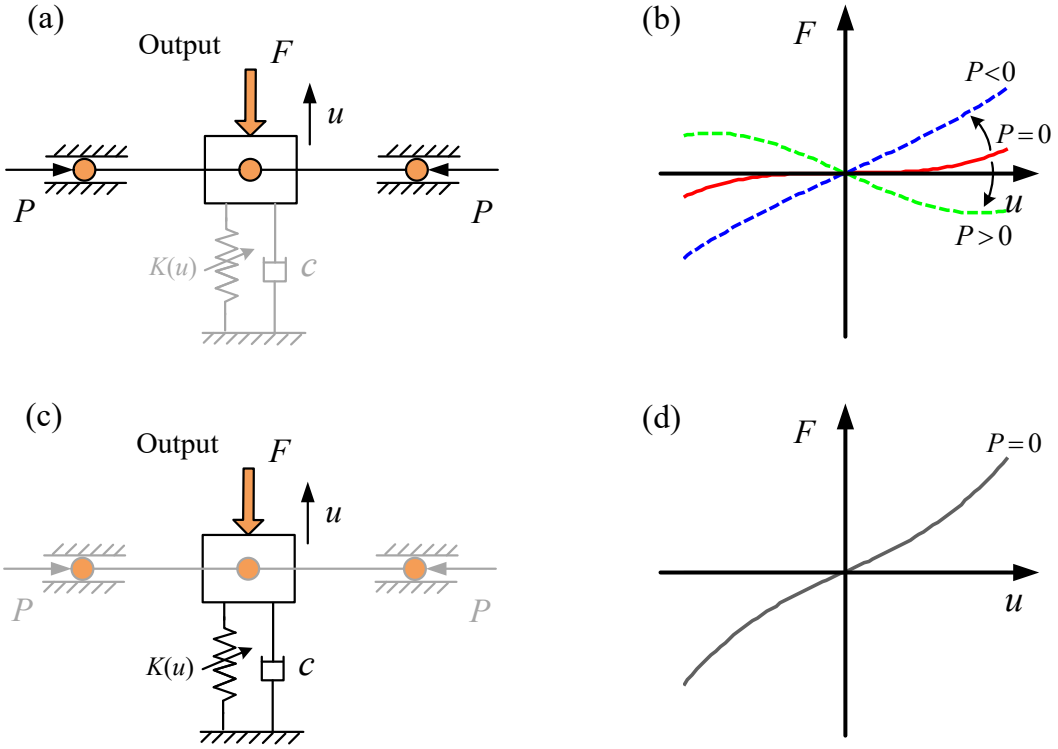

Figure 5. Schematic of the sub-system and the corresponding force-displacement curves, with respect to the compressing length: (a)(b) negative stiffness mechanism; (c)(d) nonlinear spring.

pitch. As one coil is fully compressed and becomes inactive, a transition point occurs and the spring rate increases considerably. By fitting the transition points on the objective function curve, the pitch of each coil can be calculated. However, the positions of these transition points cannot be selected, which leads to the last pitch being exceptionally large. As can be seen from Fig. 9(a), the last part is hard to fit on the objective function.

To overcome this limitation, the second type is adopted. Here, we allow some coils (usually the number is not an integer) to have the same pitch, which leads to several groups of ordinal linear springs being generated. By defining the transition points of the piecewise curve averagely on the nonlinear part, the stiffness in each piece will correspond well to the required value (see Fig. 9(b)). In this method, the number of transition points determines the number of groups possessing the same pitch. Then the number of active coils can be expressed by using the common formula:

$$n_a = \frac{\bar{G}d^4}{8D^3 \cdot k_0} \tag{19}$$

where D, d and $\bar{G}$ represent the mean diameter of the coils, the wire diameter and shear modulus of elasticity, respectively. k_0 is the initial stiffness when all coils are active, as proposed in Eq. (16). Defining the total deflection length of the spring as l_f ($l_f > 2s_t$), and the number of spring groups in nonlinear regime as n, the interval of each part in the nonlinear phase is obtained:

$$\Delta = \frac{l_f - s_t}{n} \tag{20}$$

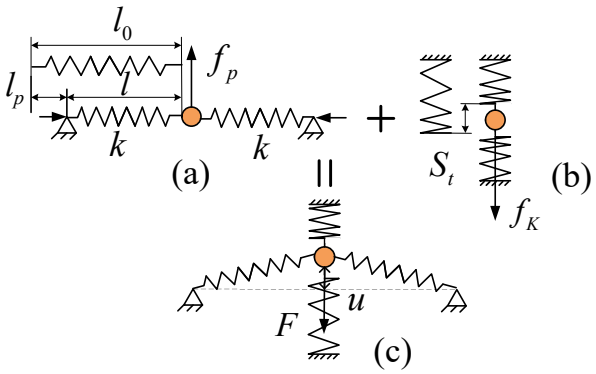

Figure 6. Detailed realization of NES system: (a) negative stiffness mechanism; (b) conical spring; (c) the composed system.

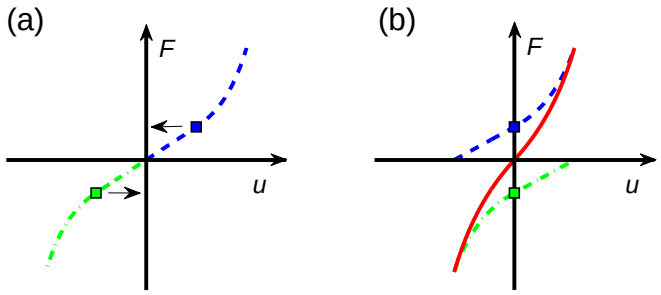

Figure 7. Force characteristics of two variable pitch springs (green and blue): (a) at original length; (b) pre-compressed at the transition point. The red curve represents the composed force.

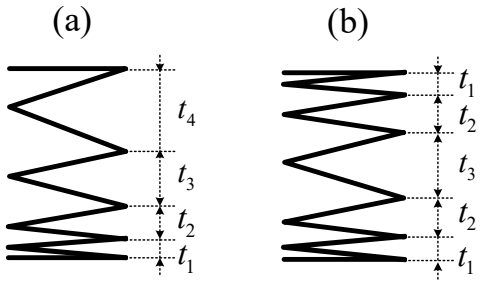

Figure 8. Two types of shape for variable pitch spring: (a) each coil with a different pitch; (b) each group of coils with a different pitch.

Within the interval of each part of the curve, the displacement and the force of each transition point are given by:

$$\begin{aligned} u_i &= s_t + i \cdot \Delta, \quad i = 1..n \\ F_i &= a_3 i^3 \cdot \Delta^3 + a_1 i \cdot \Delta + P_t \end{aligned} \tag{21}$$

Then the detailed expression of each stiffness $k_1 ... k_n$ yields:

$$k_i = \frac{F_i - F_{i-1}}{u_i - u_{i-1}} = a_3(3i^2 - 3i + 1) \cdot \Delta^2 + a_1 \tag{22}$$

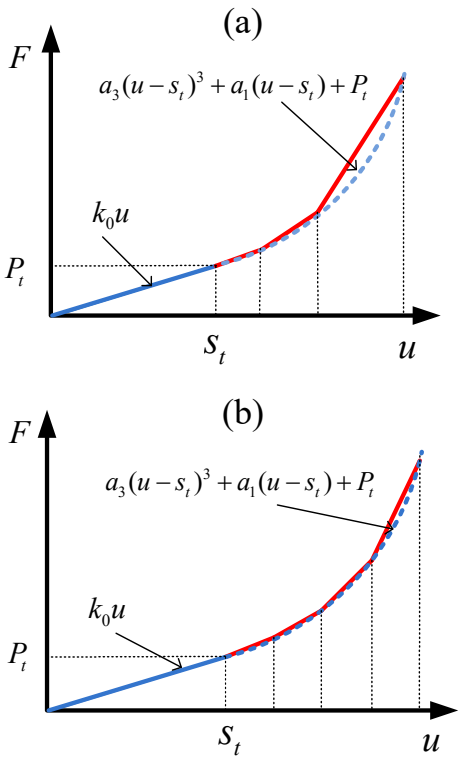

Figure 9. Force characteristics of variable pitch spring: (a) each coil with a different pitch; (b) each group of coils with a different pitch.

As the stiffness is held at k_i, the remaining active coils n_i and the number of coils in each spring group $\bar{n}_i$ can be obtained:

$$n_i = \frac{\bar{G}d^4}{8D^3 \cdot k_i}, \quad \bar{n}_i = n_{i-1} - n_i \tag{23}$$

Once the number of coils in each group has been obtained, the corresponding pitch can be calculated. When the force reaches the transition point between the linear and nonlinear parts, the first group of coils is fully compressed and its corresponding pitch is:

$$t_0 = \frac{s_t}{n} + d \tag{24}$$

When the force reaches the i_{th} transition point of the nonlinear regime, the i_{th} group of coils is fully compressed and its corresponding pitch is given by:

$$t_i = \frac{u_i - u_{i-1}}{\bar{n}_i} + t_{i-1} = \frac{\Delta}{\bar{n}_i} + t_{i-1}, \quad i = 1..n \tag{25}$$

By adding the length of each spring group to that of the closed ends, the free length of the variable pitch spring is obtained:

$$L_f = \sum_{i=1}^{n_a} n_i t_i + 1.5 \cdot d \tag{26}$$

Here, it is important to highlight that the free length should satisfy the condition: $\lambda = L_f / D \leq 2.6$, so that the variable pitch spring will not buckle as the NES mass moves in a large displacement.

Table 1. Parameters of the variable pitch spring

Objective parameters			
k_0	160 N/m	a_1	165 N/m
a_3	2.3×10^5 N/m^3	s_t	35 mm
Designed parameters			
D	40 mm	d	2 mm
G	7×10^4 Mpa	n	7
L_f	105.6 mm	n_a	13.7

Pitch parameters				
$\bar{n}_i$	t_i (mm)	α_i (^{o})	k_i (N/m)	u_i (mm)
1	4.56	2.08	160	35
2.65	5.01	2.28	173	40.75
2.96	5.59	2.55	218	46.5
2.17	6.40	2.92	309	52.25
1.42	7.57	3.45	446	58
0.93	9.23	4.20	629	63.75
0.62	11.48	5.22	857	69.5
1.93	14.45	6.56	1131	75.25

To illustrate the detailed realization of a NES system, an example of the design of a variable pitch spring is presented in Table 1. The objective parameters are achieved under a given primary system specification, and detailed process can be referred from [34]. The force-displacement equation of the variable pitch spring corresponds to Eq. (16), in which the force at the transition point is given by $P_t = k_0 s_t$. We can note that the displacement of the transition point (i.e. s_t) determines the maximum amplitude of the NES mass. The number of spring groups in the nonlinear regime (i.e. n) controls the accuracy of the curve fitting. The variable pitch characteristics are detailed in a dedicated table as follows. The columns from left to right show the number of coils, the pitch, the helix angle, the stiffness and the displacement of the corresponding transition point. As can be seen, the pitch and helix angle of each spring group increase monotonously, meaning that the pitch distribution has an ascending order. To facilitate the manufacturing process, the final pitch distribution is split to symmetrical shape, as shown in Fig. 10. With this distribution, the number of spring groups is increased but the stiffness curve keeps the same shape.

4 Experimental validation

4.1 Static test

Based on the design parameters of Table 1, the variable pitch spring was manufactured, and its force characteristics test were executed, as shown in Fig. 11(a). With this spring, a NES system providing strongly nonlinear stiffness was designed, the components of which were spherical plain bearings, a linear guide, two variable pitch springs, two linear springs and a NES mass. It is important to highlight that the distance between each spring and the NES mass was adjustable so that a suitable force shape could be reached. Details of the NES experimental setup and the measuring equipment are presented in Fig. 11(b). The NES mass was held by a ring so that it could be connected to the internal load cell of the force gauge. The force gauge has a 500 N capacity with 0.1% accuracy and 0.04 N resolution, the handle allows a stroke of 2 mm per revolution, the displacement transducer with digital display has a resolution of 0.01 mm. With this experimental setup, the force could be measured by turning the handle to control the deflection of spring.

Fig. 11 (c) and (d) show the force characteristics of the designed spring and the NES system. Based on curve fitting, polynomial parameters of the force-displacement curves are identified. Detailed comparison of parameters between the objective and static test curve is presented in Table 2. As can be seen, the manufactured spring curves and designed piecewise curve correspond to the objective curve well. The experimental curve of the NES system is close to the objective cubic curve. Thus it can be concluded that the design theory of variable pitch spring is efficient to produce the anticipated nonlinearity for the NES system. Combining variable pitch springs and a negative stiffness mechanism is a feasible way to generate pure cubic stiffness. To enable the anticipated nonlinearity to be obtained, enough pre-compressed length should be reserved in both the variable pitch and the linear springs. Moreover, buckling of the negative stiffness mechanism should not be neglected during the design procedure.

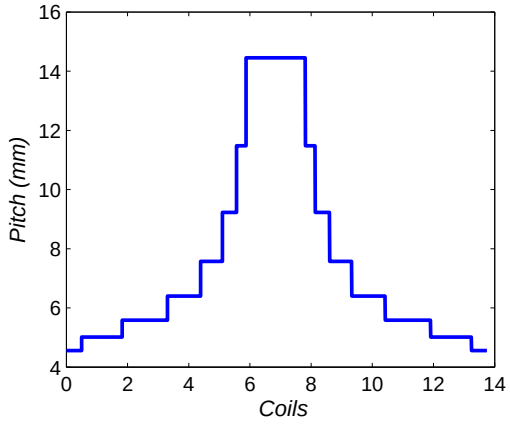

Figure 10. Symmetrical type of pitch distribution for the spring

Table 2. Comparison of parameters between design and test

Variable pitch spring $F = \begin{cases} k_0 \cdot u & (u \le s_t) \\ a_3(u-s_t)^3 + a_1(u-s_t) + P_t & (u > s_t) \end{cases}$				
	k_0 (N/m)	a_1 (N/m)	a_3 (N/m^3)	s_t (mm)
objective	160	165	2.3×10^5	35
static test	160	218	1.9×10^5	35
NES system $F = b_0 + b_1 u + b_2 u^2 + b_3 u^3$				
	b_0 (N/m)	b_1(N/m)	b_2 (N/m^2)	b_3 (N/m^3)
objective	0	0	0	4×10^5
static test	0	62	161	3.7×10^5

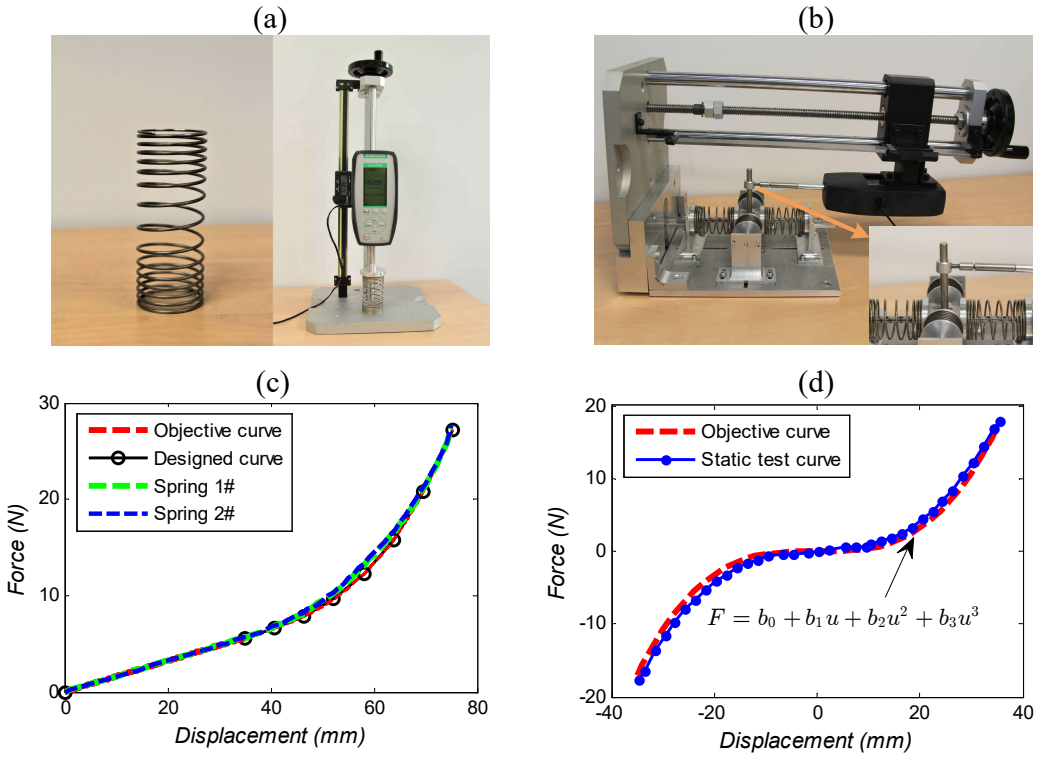

Figure 11. (a) Manufactured variable pitch spring and measuring equipment; (b) details of the NES experimental setup and measuring system; (c) force-displacement relation of the designed spring (d) force-displacement relation of the NES system.

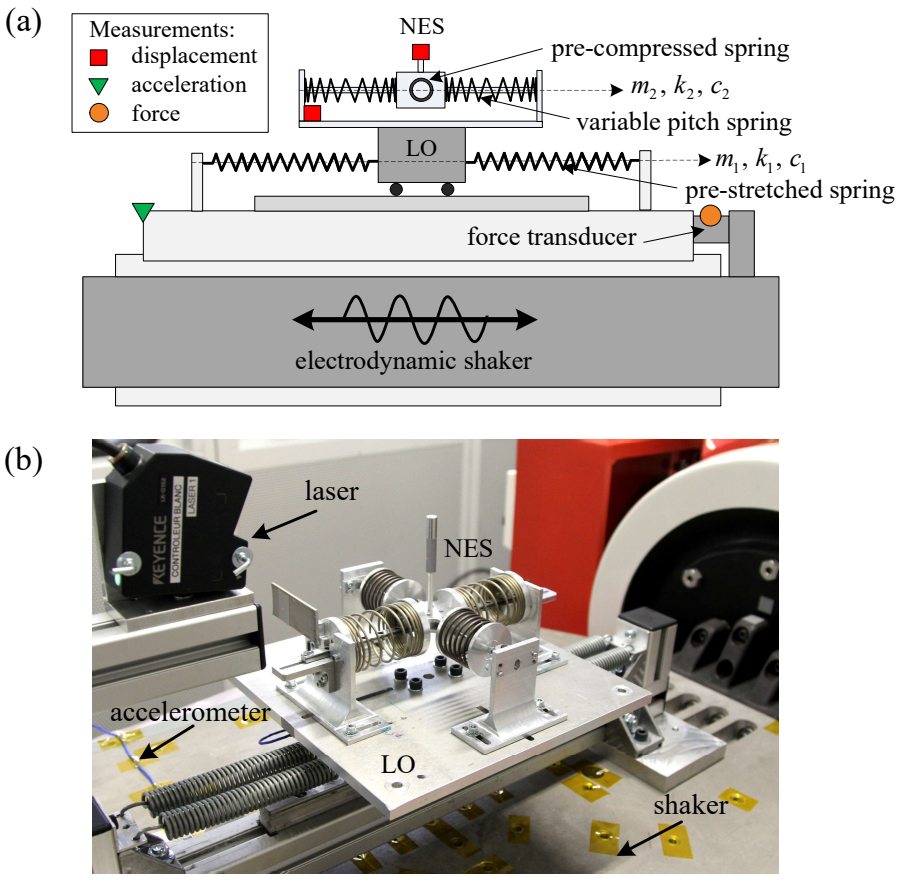

Figure 12. Experimental setup: (a) global scheme of the system and (b) detailed view of LO and NES.

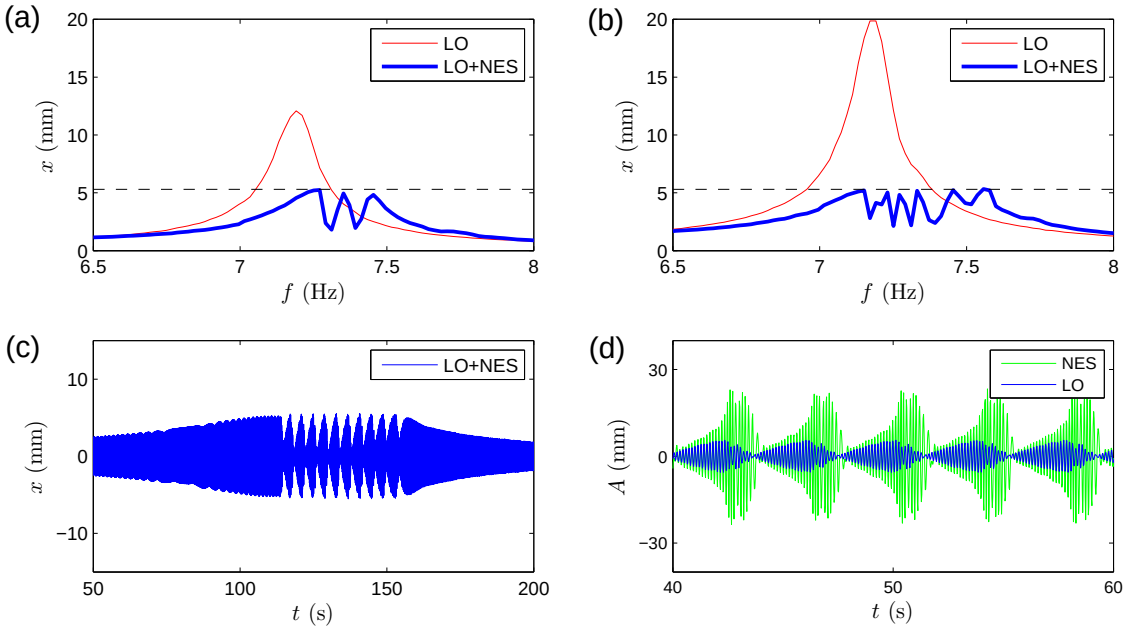

Figure 13. Experimental results: (a) frequency response curve of LO with (blue) and without (red) designed NES, $G = 0.25$ mm; (b) frequency response curve of LO with (blue) and without (red) designed NES, $G = 0.40$ mm; (c) detailed view of response of LO under frequency sweep test with $G = 0.25$ mm; (d) Strongly Modulated Response of LO (blue) and NES (green) with $G = 0.25$ mm, $\sigma = 0$.

4.2 Dynamic test

To verify the efficiency of the designed NES, an experimental study to obtain the nonlinear frequency response function of the system around the 1:1 resonance was performed. The experimental setup is presented in Fig. 12. It consisted of a linear oscillator (LO), with an embedded NES. The whole system was fixed on a 10 kN electrodynamic shaker. The displacement of the LO and NES, and the acceleration of the shaker were measured by two contactless laser displacement sensors and an accelerometer, respectively. The raw signals were recorded using a digital oscilloscope and a bandpass filter was applied to correct biases and suppress high frequency noise. The parameters of the experimental setup are given in Table 3.

The frequency response functions (FRF) under excitation with $G = 0.25$ mm and $G = 0.40$ mm are illustrated in Fig. 13 (a) and (b), respectively, where the thick blue and the thin red lines represent the response of the LO with and without the NES, x is the amplitude of LO, and A is the displacement of response under time history. It can be seen that the original peak of FRF has vanished, and the RMS value of LO amplitude is obviously decreased with vibration mitigation by the NES. As the excitation increases further, the maximum amplitude of the LO remains at the same value (5.3 mm). This result is contrary to that for the traditional linear absorber, the tuned mass damper (TMD), where the maximum amplitude of the LO is proportional to the amplitude of excitation.

The time-displacement response of a frequency sweep test under $G = 0.25$ mm is presented in Fig. 13(c). It shows that the unsmooth blue curve in Fig. 13(a) corresponds to the unstable fixed points, where a strongly modulated response (SMR) occurs. A detailed view of the SMR is presented in Fig. 13(d), where the displacements of the LO increase and decrease alternately with the cyclical activation and deactivation of the NES. In this process, targeted energy transfer (TET) occurs and the energy is irreversibly dissipated from the LO to the NES. Thus it can be concluded that this type of NES can produce energy pumping and is efficient to protect the primary system in a large band of frequencies. Moreover, it performs well in terms of controlling the maximum amplitude of the LO for different types of excitation.

Table 3. Parameters of the experiment

Physical Parameters			
m_1	5.5 kg	m_2	0.1 kg
k_1	1.15×10^4 N/m	k_2	4×10^5 N/m^3
c_1	3 Ns/m	c_2	0.4 Ns/m
Reduced Parameters			
ε	1.8%	λ_2	0.088
λ_1	0.66	K	1913

5 Conclusion

The ultimate goal of this paper is to propose a generalized methodology for designing a novel NES with variable pitch spring, so as to control the vibration of any primary system. To this end, a generic NES system including the dynamical and physical model is firstly investigated. Targeted energy transfer (TET) of a 2 DOF system comprising a harmonically

excited linear oscillator (LO) coupled with a cubic NES is studied theoretically. Strongly modulated response is shown to be beneficial for efficient TET. The physical configuration of the NES system for obtaining strongly cubic stiffness is introduced. Key features of the structure include: (i) specifically sizing two variable pitch springs to provide the force polynomial components with only linear and cubic terms; (ii) pre-compressing the two springs at the transition point to produce smooth nonlinear force characteristics; (iii) adding a negative stiffness mechanism to counterbalance the linear term. Secondly, to generate the variable pitch spring, design parametrization is implemented. Two types of shape are proposed to fit the objective force-displacement function. Among them, the type where each group of coils has a different pitch proves to produce the anticipated nonlinearity well for the NES system. Finally, a special sized NES system is developed, in which the distance between each spring and the NES mass is adjustable so that a suitable force shape can be reached. To verify the concept, identification of the force-displacement relation is performed, and a good agreement is observed between the theoretical and the experimental result. Then experiments for the whole system embedded on an electrodynamic shaker are studied. The results show that this NES is efficient to protect the primary system in a large band of frequencies. Moreover, it performs well in terms of controlling the maximum amplitude of the LO for different types of excitation, thus making it practical for the application of passive vibration control.

References

[1] Lee Y, Vakakis AF, Bergman L et al. Passive non-linear targeted energy transfer and its applications to vibration absorption: a review. *Proc Inst Mech Eng Part K J Multibody Dyn* 2008; 222(2): 77–134.

[2] Karayannis I, Vakakis A and Georgiades F. Vibro-impact attachments as shock absorbers. *Proc IMechE, Part C: J Mechanical Engineering Science* 2008; 222(10): 1899–1908.

[3] Manevitch L and Gendelman OV. Oscillatory models of vibro-impact type for essentially non-linear systems. *Proc IMechE, Part C: J Mechanical Engineering Science* 2008; 222(10): 2007–2043.

[4] Benarous N and Gendelman OV. Nonlinear energy sink with combined nonlinearities: Enhanced mitigation of vibrations and amplitude locking phenomenon. *Proc IMechE, Part C: J Mechanical Engineering Science* 2016; 230(1): 21–33.

[5] Lamarque CH, Gendelman OV, Savadkoohi AT et al. Targeted energy transfer in mechanical systems by means of non-smooth nonlinear energy sink. *Acta Mechanica* 2011; 221(1-2): 175.

[6] Su D, Zheng R, Nakano K et al. Stabilisation of the high-energy orbit for a non-linear energy harvester with variable damping. *Proc IMechE, Part C: J Mechanical Engineering Science* 2016; 230(12): 2003–2012.

[7] Su D, Nakano K, Zheng R et al. On electrical optimisation using a duffing-type vibrational energy harvester. *Proc IMechE, Part C: J Mechanical Engineering Science* 2015; 229(18): 3308–3319.

[8] Romeo F, Sigalov G, Bergman LA et al. Dynamics of a linear oscillator coupled to a bistable light attachment: Numerical study. *ASME J Comput Nonlinear Dynam* 2015; 10(1): 011007.

[9] Vakakis AF and Gendelman OV. Energy pumping in nonlinear mechanical oscillators: part ii: resonance capture. *J Appl Mech* 2001; 68(1): 42–48.

[10] Gendelman O. Targeted energy transfer in systems with external and self-excitation. *Proc IMechE, Part C: J Mechanical Engineering Science* 2011; 225(9): 2007–2043.

[11] Ahmadabadi ZN and Khadem S. Self-excited oscillations attenuation of drill-string system using nonlinear energy sink. *Proc IMechE, Part C: J Mechanical Engineering Science* 2013; 227(2): 230–245.

[12] Gourc E, Seguy S, Michon G et al. Quenching chatter instability in turning process with a vibro-impact nonlinear energy sink. *J Sound Vib* 2015; 355: 392–406.

[13] Luo J, Wierschem NE, Hubbard SA et al. Large-scale experimental evaluation and numerical simulation of a system of nonlinear energy sinks for seismic mitigation. *Engineering Structures* 2014; 77: 34–48.

[14] Luo J, Wierschem NE, Fahnestock LA et al. Realization of a strongly nonlinear vibration-mitigation device using elastomeric bumpers. *J Eng Mech* 2013; 140(5): 04014009.

[15] Wang J, Wierschem NE, Spencer Jr BF et al. Track nonlinear energy sink for rapid response reduction in building structures. *J Eng Mech* 2015; 141(1): 04014104.

[16] Kani M, Khadem SE, Pashaei MH et al. Design and performance analysis of a nonlinear energy sink attached to a beam with different support conditions. *Proc IMechE, Part C: J Mechanical Engineering Science* 2016; 230(4): 527–542.

[17] McFarland DM, Bergman LA and Vakakis AF. Experimental study of non-linear energy pumping occurring at a single fast frequency. *Int J Non-Linear Mech* 2005; 40(6): 891 – 899.

[18] Mariani R, Bellizzi S, Cochelin B et al. Toward an adjustable nonlinear low frequency acoustic absorber. *J Sound Vib* 2011; 330(22): 5245–5258.

[19] Gourc E, Michon G, Seguy S et al. Experimental investigation and design optimization of targeted energy transfer under periodic forcing. *ASME J Vib Acoust* 2014; 136(2): 021021.

[20] Wahl AM. *Mechanical springs*. Penton Publishing Company, 1944.

[21] Paredes M and Rodriguez E. Optimal design of conical springs. *Engineering with computers* 2009; 25(2): 147.

[22] Jutte CV and Kota S. Design of single, multiple, and scaled nonlinear springs for prescribed nonlinear responses. *ASME J Mech Des* 2010; 132(1): 011003.

[23] Paredes M. Analytical and experimental study of conical telescoping springs with nonconstant pitch. *ASME J Mech Des* 2013; 135(9): 094502.

[24] Wang H, He P, Pang B et al. A new computational model of large three-row roller slewing bearings using nonlinear springs. *Proc IMechE, Part C: J Mechanical Engineering Science* 2017; 231(20): 3831–3839.

[25] Wu YS and Lan CC. Linear variable-stiffness mechanisms based on preloaded curved beams. *ASME J Mech Des* 2014; 136(12): 122302.

[26] Sönmez Ü and Tutum CC. A compliant bistable mechanism design incorporating elastica buckling beam theory and pseudo-rigid-body model. *ASME J Mech Des* 2008; 130(4): 042304.

[27] Chen YH and Lan CC. An adjustable constant-force mechanism for adaptive end-effector operations. *ASME J Mech Des* 2012; 134(3): 031005.

[28] Stanton SC, McGehee CC and Mann BP. Nonlinear dynamics for broadband energy harvesting: Investigation of a bistable piezoelectric inertial generator. *Physica D: Nonlinear Phenomena* 2010; 239(10): 640–653.

[29] Al-Shudeifat MA. Nonlinear energy sinks with nontraditional kinds of nonlinear restoring forces. *ASME J Vib Acoust* 2017; 139(2): 024503.

[30] Gendelman O, Starosvetsky Y and Feldman M. Attractors of harmonically forced linear oscillator with attached nonlinear energy sink i: Description of response regimes. *Nonlinear Dyn* 2008; 51(1): 31–46.

[31] Vakakis AF, Gendelman OV, Bergman LA et al. *Targeted Energy Transfer in Mechanical and Structural Systems*, volume 156. Springer Science & Business Media, Berlin, 2008.

[32] Nayfeh AH. *Introduction to perturbation techniques*. John Wiley & Sons, 2011.

[33] Starosvetsky Y and Gendelman O. Strongly modulated response in forced 2dof oscillatory system with essential mass and potential asymmetry. *Physica D: Nonlinear Phenomena* 2008; 237(13): 1719–1733.

[34] Qiu D, Seguy S and Paredes M. Tuned nonlinear energy sink with conical spring: Design theory and sensitivity analysis. *ASME J Mech Des* 2018; 140(1): 011404.